Gas Processing Journal

Vol. 9, No. 1, 2021, pp. 141 - 156
http://gpj.ui.ac.ir

Research Paper

Thermodynamic evaluation of a novel solar-aided biogas polygeneration system integrated with steam network

Hossein Nikoomaram [1], Majid Amidpour [*2], Mostafa Panahi [3], Amir Farhang Sotoodeh[3]

[1] Department of Energy Engineering, Faculty of Natural Resource and Environment, Science and Research Branch, Islamic Azad University, Tehran, Iran
[2] Department of Energy System Engineering, Faculty of Mechanical Engineering, K. N. Toosi University of Technology, No. 15, Pardis St., Molasadra Ave., Vanak Sq., Tehran, Iran
[3] Energy and Environment Faculty, Niroo Research Institute (NRI), Tehran, Iran

Received: 2021-06-20 Revised: 2021-09-08 Accepted: 2021-10-02

Abstract: The limited resources of fossil fuel and environmental concerns necessitate utilizing renewable resources which are less environmentally harmful. A new cogeneration system integrated with CCS and hydrogen production units is developed and analyzed in detail by introducing biogas and solar energy. The proposed system is presented to provide the heating demand of a utility system by designing a proper heat recovery. Concentrated solar thermal (CST) tower, biogas reformer, gas turbine cycle (GTC), organic Rankine cycle (ORC), pressure swing adsorption (PSA), carbon capture and storage (CCS) as the topping system and steam network (SN) are the components of this system. The devised system is evaluated from the energy point of view. A comprehensive parametric analysis is conducted for assessing the impact of the main parameters. The results demonstrate that integrating the SN and topping system increases the energy efficiency from 51.72% to 60.55%. Consequently, the net power generated by the system is increased from 32.147 MW to 57.634 MW.

keywords: Biogas reformer; Carbon capture and storage; Cogeneration; Steam network; Solar energy.

Nomenclature

Symbols

A	Area (cm^2)
C_r	Concentration ratio
d	Diameter
D	Extent of reforming reactions (kmol s^{-1})
DNI	Direct normal irradiation (W m^{-2})
Fr	View factor
$\Delta\bar{G}^0$	Gibbs free energy ($kJkmol^{-1}$)
h	Specific enthalpy ($kJkg^{-1}$)
$\hat{h}$	Convective heat transfer coefficient ($wm^{-1}k^{-1}$)
$\bar{h}_f^0$	Enthalpy of formation ($kJkmol^{-1}$)
h	Specific enthalpy ($kJkg^{-1}$)
k	Thermal conductivity ($wm^{-1}k^{-1}$)
K_p	Equilibrium constant
l	Height of receiver aperture (m)
LHV	Low heating value ($kJkg^{-1}$)
$\dot{m}$	Mass flow rate (kg s^{-1})

Greek symbols

η	efficiency (%)
μ	Dynamic viscosity (Pa s)
θ	Solar incident angle (deg)
ρ	Density (kgm^{-3})

Subscripts and superscripts

0	Ambient
abs	Activation
ap	Actual
comp	Compressor
cog	Cogeneration
D	Destruction
eq	Equilibrium
el	Electrical
en	Energy
G	Generator
is	Isentropic

* **Corresponding Author.**
Authors' Email Address: [1] **H. Nikoomaram** (nikomaram1380@gmail.com), [2] **M. Amidpour** (amidpour@kntu.ac.ir), [3] **M. Panahi** (mpstudents.2020@gmail.com), [4] **A. F. Sotoodeh** (asotoodeh@nri.ac.ir)

DOI: http:// 10.22108/GPJ.2021.129187.1104

N	Number of receiver tubes
$\dot{N}$	Molar rate (kmol s^{-1})
Nu	Nusselt number
P	Pressure (bar)
Pr	Prandtl number
$\dot{Q}$	Heat rate (kW)
R	Net power/heating ratio
$\overline{R}$	Universal gas constant (=8.314 kJ $kmol^{-1}K^{-1}$)
R_e	Reynolds number
s	Specific entropy ($kJkg^{-1}K^{-1}$)
$\bar{s}$	Absolute entropy ($kJkmol^{-1}K^{-1}$)
T	Temperature (K)
V	Velocity (m s^{-1})
w	Width of receiver aperture (m)
$\dot{W}$	Power (kW)
X	Molar concentration

i	i^{th} component
ms	Molten salt
r	Reformer
rec	Receiver
sur	Surface
T	Target
th	Thermal

Abbreviations

ADP	Acid dew point
BFW	Boiler feed water
CST	Concentrated solar thermal
CHP	Combined heat and power
CC	Combustion chamber
CCS	Carbon capture and storage
DR	Dry reforming reaction
DWH	Domestic water heater
FG	Flue gases
GLS	Gas-liquid separator
GT	Gas turbine
GTC	Gas turbine cycle
HP	High pressure
HRSG	Heat recovery steam generator
LP	Low pressure
MSR	Methane/steam reforming reaction
MP	Medium pressure
ORC	Organic Rankine cycle
PSA	Pressure swing adsorption
RWGS	Reverse water gas shift
SN	Steam network
ST	Steam turbine
VHP	Very high pressure
WGS	Water/gas shift reaction

Introduction

Carbon dioxide emission via the combustion of conventional energy sources has the most contribution to the global climate crises including global warming and environmental degradation [1, 2]. On the other hand, energy efficiency plays an essential role in sustainability development [3]. Thus, renewable-based polygeneration set-ups are becoming more and more desirable and attractive [4]. Polygeneration systems serve as an offering energy-efficient technology which delivers different types of energy carriers in a specific integrated complex simultaneously [5].

Among renewable resources, solar energy is the most promising one since it is available, clean, secure, and economical [6]. It can be employed in polygeneration systems as the main source of energy including thermal collectors and photovoltaic panels. Particularly, different types of solar technologies are available which can be utilized in polygeneration set-ups for the direct conversion of the sun irradiation at various operating temperatures [7]. For instance, in low- and mid-temperature ranges, the generated heat is utilized in heating and cooling applications mostly. Solar heating and cooling technologies, which convert the sun's rays into space heating and cooling, are considered more attractive in summer since the cooling demand is frequently concurrent to the available solar intensity [8]. In high-temperature levels, the produced heat is introduced to power plants for power generation along with other useful products [9, 10].

The agricultural and animal wastes could be used as a primary feedstock for energy production [11, 12]. In recent years, these organic materials have been implemented for biogas production which includes methane and carbon dioxide. Using biogas containing carbon dioxide is not favorable in fuel cells and combustible engines. For this matter, biogas is often converted to a mixture of carbon monoxide and hydrogen through a reformer. Two kinds of reforming reactions take place during this process which are endothermic and exothermic. Furthermore, in this way, the produced gas is improved because of the achieved hydrogen via the biogas reforming biogas [13]. In the last decade, many studies discussed different approaches for biogas reforming, according to the nature of energy system [14].

Multi-generation mostly indicates that power and valuable heat are produced at the same time,

along with other products, which is conceivable by employing the additional surplus heat that would be wasted in conventional systems. In this regard, Mouaky and Rachek [15] suggested a novel hybrid polygeneration system based on solar and biomass which is capable of producing power, heating, cooling, and freshwater for a residential area with forty households.

Polygeneration has a wide-range of applications including utilities, buildings sectors, as well as in different industrial clusters such as pulp, plastic, agriculture, and chemical [16, 17]. Numerous studies have investigated a variety of polygeneration systems [18-20]. For instance, Bai et al. [21] proposed a solar-biomass gasification system consisting of a biomass-steam gasification and concentrated solar thermal (CST) tower power generation system for methanol and electricity production. The reported exergy efficiency of the proposed configuration was 51.23%.

Above all, using solar energy as the heat source has been considered a promising technology for polygeneration systems. In recent years, utilizing solar energy as upstream in polygeneration systems has been increased. In the present paper, a new polygeneration system with the combination of CST tower, biogas-steam reformer, steam network (SN), pressure swing adsorption (PSA), carbon capture and storage (CCS), gas turbine cycle (GTC), and organic Rankine cycle (ORC) has been studied from a thermodynamic viewpoint. A review of the literature shows the lack of research on the integration of renewable resources and utility steam networks for heat recovery purposes. Due to the importance of this area, this paper aims to investigate the cogeneration efficiency of the devised configuration. Also, the impacts of key parameters are assessed through a parametric study.

2. Systems description

The graphical representation of the proposed system with hydrogen production and carbon capturing is demonstrated in Fig. 1. The system includes a CST tower plant, a biogas-steam reformer, an SN, a PSA, a CCS, a GTC, and an ORC. The description of this setup is shown below.

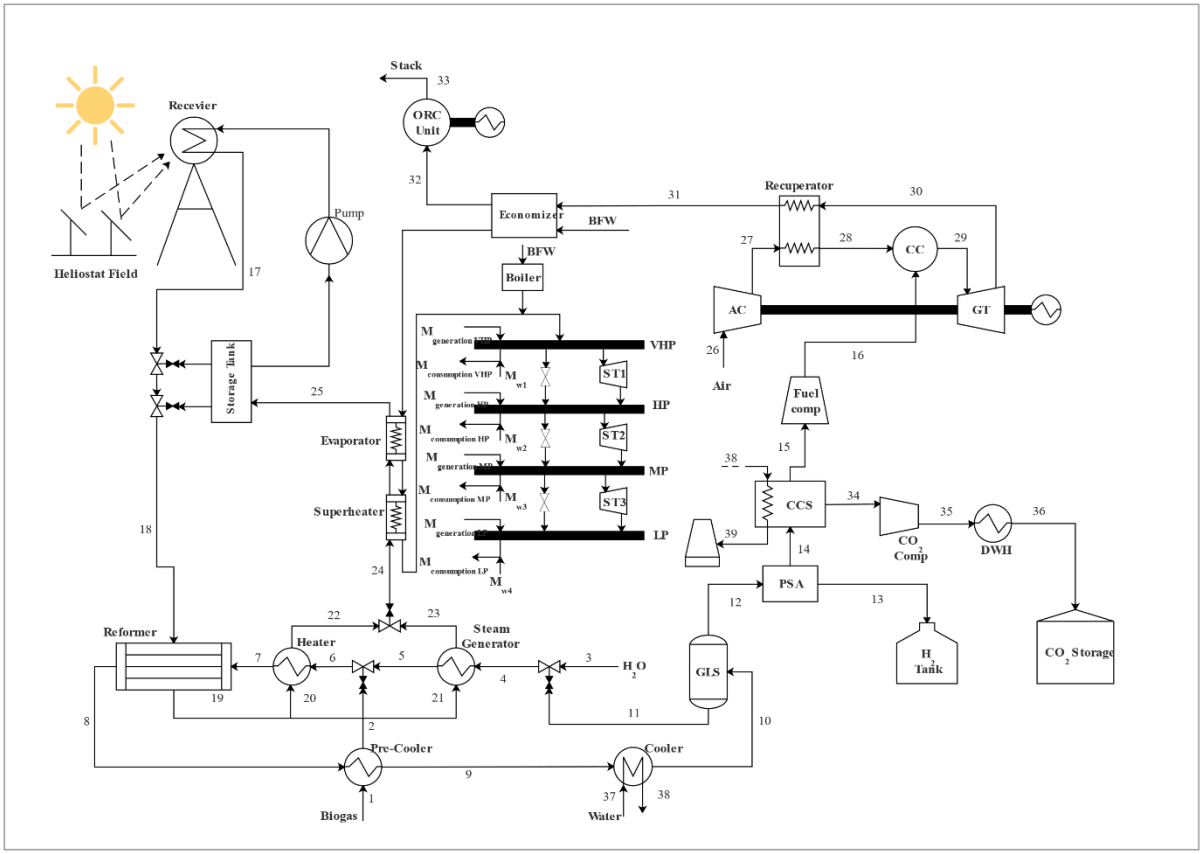

Figure 1 Graphical representation of the proposed hybrid integrated set-up.

In this paper, Solar energy provides the reforming heat requirement and also runs the steam network. This CST tower plant comprises a receiver, heliostat fields, and a thermal storage unit. The heliostats track and concentrate the sun's beams to a focal point which is situated on the apex of the heliostat field. Thermal energy storage is also implemented to deposit a surplus of thermal energy. The produced high-temperature molten salt flows through a reformer (state 18) to deliver the required heat for reforming reactions. In-state 3, water is mixed with condensed water

from a gas-liquid separator (GLS) (state 11). The produced steam is mixed with reformed biogas. The required thermal energy for CO_2 capturing is provided by the heat that is absorbed from water at state 39. At state 10, the low-temperature syngas flows through the GLS where the condensed water splits (state 11). Later, the reformed biogas with low-content of H_2O (state 12) moves into the PSA and CCS.

The SN unit comes with three modular heat exchangers, including an economizer, an evaporator, and a superheater. The function of NG is to be used as a fuel to deliver a surplus amount that is needed by modular heat exchangers for steam production and heating. The exploitation of the CCS unit in power plants has led to a great reduction in CO_2 emission. Based on the work published by Van-Dal and Bouallou [22], the CCS unit utilized in this study uses monoethanolamine (MEA) as a solvent with a mass concentration of 30%. Their results show that the CO_2 capture rate of devised CCS module is 85% while the energy consumption for feed compression is 44 kWh_{el} per tons of CO_2. In addition, the energy needed for solvent regeneration is 3200 kJ/kg of CO_2, and the pressure drop occurring in this unit is around 5%.

In GTC, Inlet air is passed through an air compressor (AC) and then a recuperator is utilized for preheating this compressed air (state 28). Leaving the CCS at state 16, the unreacted syngas and hot air are guided into a combustion chamber (CC) in order to be burnt. Afterward, the hot flue gas is implemented for heating the compressed air in a recuperator (state 30). Also, the boiler feedwater (BFW) in the economizer (state 31) is heated by recovering heat from the flue gas. In this paper, a toluene-based organic ranking cycle (ORC) is used, which is integrated with an internal heat exchanger [23]. The Toluene of the ORC evaporator retrieves waste heat within the flue gas exiting the economizer. The saturated vapor of the toluene is utilized for producing power through a turbine. Then the thermal energy of the toluene, which exits the turbine is exploited by a recuperator. Afterward, this energy is transported to the toluene stream, which is introducing into the evaporator. The cooling water is used to cool the ORC turbine outlet stream and turning it into saturated liquid in the condenser.

3. Methodology

In this paper, the devised system is analyzed and evaluated from the thermodynamic point of view. The assumptions used in this evaluation are as follow [24, 25]:

- A steady-state model is applied for scrutinizing each sub-system.
- Potential and kinetic energy effects are ignored.
- Heat loss in heat exchangers and pipelines is neglected.
- For steam turbines of the SN unit, a variable isentropic efficiency is considered.
- Water is employed for desuperheating the deaerator steam.
- Acid dew point at 120℃ temperature is assumed for flue gas.
- The pressure of deaerators is presumed 1.208 bar.
- Steam flew through steam generation part is superheated.
- The value of pressure drop in the heat exchangers is considered 1% and 2% hot and cold sides, respectively.
- PSA unit recovers Hydrogen content from syngas up to 85%. The cross-sectional area of this unit is 1.6 cm^2, and according to literature, and its pressure drop is about 2.5% [26, 27].

The general mass and energy balances equations for these components in a volume control are as follow [28, 29]:

$$\sum_i \dot{m}_{\text{inlet}} - \sum_i \dot{m}_{\text{outlet}} = 0$$

$$\dot{Q} - \dot{W} = \sum_i (\dot{m}h)_{\text{outlet}} - \sum_i (\dot{m}h)_{\text{inlet}}$$

3.1. Solar system

The heliostat field consisted of several heliostats with total aperture area (A_{field}) is considered in this study. The following equations are used for scheming the concentrated solar energy [30]:

$$Q_{field} = DNI.A_{field}$$

After calculating Q_{field}, total indication absorbed energy is computed using Eq. (4).

$$Q_{rec,in} = \eta_{field} \times Q_{field}$$

The following relation demonstrates the total energy balance for the molten salt cavity receiver. In Eq. (5), Q_{abs} denotes the net energy absorbed by the receiver and $Q_{total,loss}$ is the total of heat losses:

$$Q_{rec,in} = Q_{total,loss} + Q_{abs}$$

The relation between the average temperature of the receiver surface ($T_{rec,sur}$) and the average molten salt temperature (T_{ms}) is illustrated by Eq. (6) [30]:

$$q_{rec,in} = \frac{T_{rec.sur} - T_{ms}}{\frac{d_o}{d_i h_{ms}} + \frac{d_o}{2\gamma_{rec,tube}} ln\frac{d_o}{d_i}} = \frac{Q_{rec,in}}{A_{rec,sur}}$$

$$T_{ms} = \frac{T_{rec,out} + T_{rec,in}}{2}$$

Li et al. [31] applied the Dittus–Boelter equation for computing the convective heat transfer coefficient of molten salt:

$$Nu_{ms} = 0.023 \times Re_{ms}^{0.8} \times Pr_{ms}^{0.4} = \frac{\hat{h}_{ms} \times d_i}{k_{ms}} \quad (8)$$

Where,

$$Re_{ms} = \frac{4 \times \dot{m}_{ms}}{\pi \times N_{rec,tube} \times d_i \times \mu_{ms}} \quad (9)$$

$$Fr = \frac{A_{rec,ap}}{A_{rec,sur}} \quad (10)$$

$$A_{rec,ap} = H \times W \quad (11)$$

$$C = \frac{A_{field}}{A_{rec,ap}} \quad (12)$$

Where F_r denotes the view factor and C_r is the concentration ratio.

The receiver aperture width is presumed $0.5H$ [30]. The absorbed receiver energy should provide the required heat energy for biogas reforming:

$Q_{abs} = Q_{bio,ref} = \dot{m}_{ms}\,(T_8 - T_7)$

Then, the relationship among a number of receiver tubes and molten salt flowrate could be described as:

$$N_{rec,tube} = \frac{4\dot{m}_{ms}}{\rho_{ms} \times V_{max,ms} \times \pi \times d_i^2}$$

In this paper, the molten salt concludes of KCl/MCl_2 (62/38 w/w) is used as heat transfer fluid [32]. The required data for solar system modeling are listed in Table 1.

Table 1: Main parameters for simulation of the CST tower [30, 32]

Parameter	Value
Direct normal irradiation, DNI (W m^{-2})	900
Concentration ratio, C (-)	900
View factor, Fr (-)	0.8
Receiver inlet temperature, T_{25} (°C)	286
Receiver outlet temperature, T_{17} (°C)	565
Heliostat field efficiency, η_{field} (%)	60
Maximum molten salt velocity in receiver tube, $V_{max,ms}$ (ms^{-1})	4
Receiver tube outside diameter, d_o (m)	0.04
Receiver tube inside diameter, d_i (m)	0.0375
Dynamic viscosity, μ_{ms} (kg m^{-1} s^{-1})	0.00326
Density, ρ_{ms} (kg m^{-3})	1820
Specific heat capacity, C_p (J kg^{-1} K^{-1})	1553
Thermal conductivity, k_{ms} (W m^{-1} K^{-1})	0.52

3.2. Biogas-Steam reformer

Since direct use of biogas in gas turbines and combustion engines is low-efficient and environmentally hazardous, an alternative method should be devised as a replacement for the utilization of biogas directly. Dry reforming (DSR), methane CO_2 reforming, and methane steam (MSR) reforming are among the main reactions of the reforming process. There are also secondary reactions such as water gas shift (WGS), which are of high importance to produce high-quality syngas and decrease CO_2 greenhouse gas emissions [33]. These reactions could be described as below [34]:

Methane CO2 reforming: $CH4 + CO2 \rightarrow 2CO + 2H2 \quad \Delta H^0_{298K} = 247.025$ kJ/mol (15)

Methane steam reforming: $CH4 + H2O \rightarrow CO + 3H2 \quad \Delta H^0_{298K} = 205.878$ kJ/mol (16)

Water Gas Shift: $CO + H2O \rightarrow CO2 + 3H2 \quad \Delta H^0_{298K} = -41.146$ kJ/mol (17)

Total reaction: $CH4 + 2H2O = CO2 + 4H2 \quad \Delta H^0_{298K} = 164.732$ kJ/mol (18)

The following relations are the equations for the molar flow rate in the reformer outlet:

$\dot{N}_8^i = \dot{N}_8^i + d^i$ (13)

$d^{CH4} = -D_{dr} - D_{sr}$

$d^{CO2} = -D_{dr} + D_{wgs}$

$d^{CO} = -2D_{dr} + D_{sr} - D_{wgs}$ (14)

$d^{H2O} = -D_{sr} - D_{wgs}$

$d^{H2} = 2D_{dr} + 3D_{sr} + D_{wgs}$

D_{dr}, D_{sr}, D_{wgs} denote the extents of reactions presented in Eqs. (19)-(24), respectively. Also, the equilibrium compositions at the expense of the reformer can be described in the following:

$X_{eq}^i = \dot{N}_8^i / \dot{N}_8$ where $\sum X_{eq}^i = 1$

In order to calculate unknown parameters, the following relations can be applied:

$$K_{p,dr} = \exp\left(\frac{-\Delta\bar{G}^0_{dr}}{\bar{R}T_r}\right) = \frac{(X_{eq}^{CO})^2(X_{eq}^{H_2})^2}{(X_{eq}^{CH_4})(X_{eq}^{CO_2})} \times \left(\frac{P_r}{P_0}\right)^2 \quad (26)$$

$$K_{p,sr} = \exp\left(\frac{-\Delta\bar{G}^0_{sr}}{\bar{R}T_r}\right) = \frac{(X_{eq}^{CO})(X_{eq}^{H_2})^3}{(X_{eq}^{CH_4})(X_{eq}^{H_2O})} \times \left(\frac{P_r}{P_0}\right)^2 \quad (27)$$

$$K_{p,wgs} = \exp\left(\frac{-\Delta\bar{G}^0_{wgs}}{\bar{R}T_r}\right) = \frac{(X_{eq}^{CO_2})(X_{eq}^{H_2})}{(X_{eq}^{CO})(X_{eq}^{H_2O})} \quad (28)$$

$$\Delta\bar{G}^0 = \sum \bar{h}_f^0 + (\bar{h}_T - \bar{h}_{298\,K}) - T_r\bar{s} \quad (29)$$

Where, $\bar{R}$ and $\Delta\bar{G}^0$ are the universal gas constant, $\bar{h}_f^0$ and $\Delta\bar{G}^0$ Gibb's free energy in kJ $kmol^{-1}$, respectively. Table 2 tabulated the main input parameters for the biogas reforming [25].

Table 2: Main parameters for simulation of the biogas-steam reformer [25]

Parameters	Value
Inlet mass flow rate, $\dot{m}_1$ (kg)	0.305
Steam to carbon ratio (S/C)	1
Inlet CH_4 to CO_2 ratio	60/40
Inlet temperatures of water and biogas, $T_{1,3}$ (°C)	25
Reformer temperature, T_8 (°C)	750
Operating pressure, P_r (bar)	1
Reaction side pressure drop (%)	10
Inlet temperature of syngas to GLS, T10 (K)	308

3.3. Gas turbine cycle

The following reaction equation describes the basis of complete combustion with excess air:

$$(\dot{N}_{16}^{CH_4})CH_4 + (\dot{N}_{16}^{CO})CO + (\dot{N}_{16}^{CO_2})CO_2 + (\dot{N}_{16}^{H_2})H_2 + (\dot{N}_{16}^{H_2O})H_2O + (\dot{N}_{26}^{air})(0.21O_2 + 0.79N_2) \rightarrow (\dot{N}_{29}^{CO_2}CO_2 + \dot{N}_{29}^{H_2O}H_2O + \dot{N}_{16}^{N_2}N_2 + \dot{N}_{16}^{O_2}O_2)_{flue\ gass} \quad (30)$$

A recuperator is designed for preheating the air that flows through the combustion chamber. The following relation is applied for computing the temperature of the compressed air [35]:

$$T_{27}/T_{26} = 1 - \frac{1}{\eta_{is,AC}}\left[\left(\frac{P_{27}}{P_{26}}\right)^{\frac{\gamma-1}{\gamma}} - 1\right] \quad (31)$$

Also, the flue gas temperature can be determined as follows:

$$T_{30}/T_{29} = 1 - \eta_{is,GT}\left[1 - \left(\frac{P_{29}}{P_{30}}\right)^{\frac{1-\gamma}{\gamma}}\right] \quad (32)$$

Where, $\eta_{is,GT}$ signifies the isentropic efficiency, and γ is the specific heat ratio. Consequently, Eq. (33) is used for calculating the net electricity:

$$\dot{W}_{el,GTC} = \eta_G(\dot{W}_{GT} - \dot{W}_{AC}) \quad (33)$$

In this relation, η_G denotes the generator efficiency. Table 3 presented the key input parameters of the GTC.

Table 3: Main parameters for simulating the GTC [25, 36]

Parameters	Value
Ambient temperature, T_0 (K)	298
Ambient pressure, P_0 (bar)	1
Pressure ratio of air compressor	10
Gas turbine isentropic efficiency (%)	88
Air compressor isentropic efficiency (%)	83
Fuel compressor isentropic efficiency (%)	80
Generator efficiency (%)	90
Pressure drop of combustion chamber (%)	2
Inlet temperature of gas turbine (K)	1200
Effectiveness of recuperator (%)	90
Outlet stack temperature (K)	430

3.4. Steam network modeling

3.4.1 heat recovery unit

In this paper, a series of heat exchangers including an economizer, an evaporator, and a superheater is developed which functions as an HRSG. In modeling an HRSG unit, the most crucial point that should be considered is avoiding a drop of the outlet gas temperature below the acid dew point, because this incident can result in deterioration of the equipment. The following relation is utilized for calculating the amount of heat retrieved from the flue gases by an HRSG unit [37]:

$$\dot{m}_{BFW}(h_{VHP} - h_{BFW}) = \eta_{HRSG}\dot{m}_{FG}(C_{FG,in}T_{FG,in} - C_{FG,ADP}T_{FG,ADP}) \quad (34)$$

where,

$$C_{P,FG} = \sum x_i C_{p,i} \quad (35)$$

In these relations, η_{HRSG} means the thermal efficiency of the HRSG unit, and its presumed value is 90% [37].

Based on the amount of fuel and flue gas entered into the HRSG, the enthalpy of the inlet gas of the superheater can be utilized for determining the amount this necessitated extra fuel:

$$\dot{m}_{FG}h_{FG} + \dot{m}_{NG}LHV_{CH_4} = (\dot{m}_{FG} + \dot{m}_{NG})h_{GM} + (1 - \eta_{DB})\dot{m}_{NG}LHV_{CH_4} \quad (36)$$

In this relation, η_{DB} is the efficiency of the duct burner (DB), which is assumed to be 93% [37]. Due to its small extracted power, the pump work is ignored.

3.4.2. Steam turbine

The following formula gives the flow rate of steam going through a turbine at each step:

$$\dot{m}_{level\ i} = \dot{m}_{steam\ turbine,input} - \sum_{j<i}\dot{m}_{j,output} + \sum_{j<i}\dot{m}_{j,input} \quad (37)$$

According to Ref. [38], the following relation shows the relationship of the maximum isentropic power and the shaft power of the turbine at the full turbine load.

$$W_{IS,max} = aW_{max} + b \quad (38)$$

Therefore, the steam turbine efficiency at maximum loading can be calculated by the following relation:

$$\eta_{ST,max} = \frac{1}{a + \frac{b}{W_{max}}} \quad (39)$$

The maximum mass flow streaming in the steam turbine can be utilized for calculating steam turbine efficiency as the following relation presents [38]:

$$\eta_{ST,max} = \frac{1}{a}\left(1 - \frac{b}{m_{max}\Delta H_{IS}}\right) \quad (40)$$

Which a and b are calculated as follows

$$a = a_1 + a_2P_{in} + a_3P_{out} \quad (41)$$

$$b = b_1 + b_2P_{in} + b_3P_{out} \quad (42)$$

In the above relations, P_{in} and P_{out} are the inlet are the pressures of the entering and exiting steam, respectively. The coefficients a and b can be found in Table 4 [38].

Table 4: Necessary coefficients used in Eqs. (41-42) [38].

Constants	Back-pressure turbines
$a1$	1.1880
$a2$	-2.9564×10^{-4}
$a3$	4.6473×10^{-3}
$b1$	449.98
$b2$	5.6702
$b3$	−11.505

3.4.3. Steam network targeting

After developing the network, the system could have the maximized mass flow rate of the steam passing from each turbine. Consequently, the mass flow rate of steam from each steam header to another is presumed to vanish completely. By investigating the potential of power generation when the power network is functioning adequately, the fuel consumption of the system can be appropriately targeted. In order to reach this target, the system should be designed in a way that sets the mass flow variation in each header in accordance with the degree of superheating of each header. In the targeting of each header, the mass balance equation can be used to calculate the flow rate of steam passing from each turbine. The relation is as follows [24]:

$$\sum \dot{m}_{Turbine} + \sum \dot{m}_{Letdown\ Station} + \dot{m}_{Steam\ Generation} - \dot{m}_{Steam\ Use} = 0 \quad (43)$$

After calculating the mass flow rate of steam passing through the turbine, the energy balance can be employed to the low-pressure header in order to determine the steam enthalpy at the outlet of the turbine (or at the inlet of the low-pressure header) [38]:

$$h_{Turbine,input} + \dot{m}_{Turbine,intput} + h_{Letdown\ Station,input}\dot{m}_{Letdown\ Station,input} + h_{\ Steam\ Generation}\dot{m}_{Steam\ Generation} = h_{header}\left(\dot{m}_{Steam\ Generation} + \dot{m}_{Turbine,input} + \dot{m}_{Letdown\ Station,input}\right) \quad (44)$$

According to Ref. [24], the enthalpy at the outlet of the steam turbine can be determined after computing the maximum steam turbine efficiency using the following formula:

$$h_{out} = h_{in} - \frac{W}{\eta_{ST,max} m_{max}} \quad (45)$$

After determining the enthalpy, the new header temperature should be used for re-targeting steam consumption and achieving updated values of steam mass flow rate. This process is iterated until finding out the required properties at all headers. Throughout calculating the steam temperature at the high pressure, the temperature should not exceed the tolerable limit for the steam network system (570℃). A trial-and-error approach should be used in this process until the fulfillment of the constraints. Fig. 2. illustrates the targeting algorithm for the cogeneration system in the steam network.

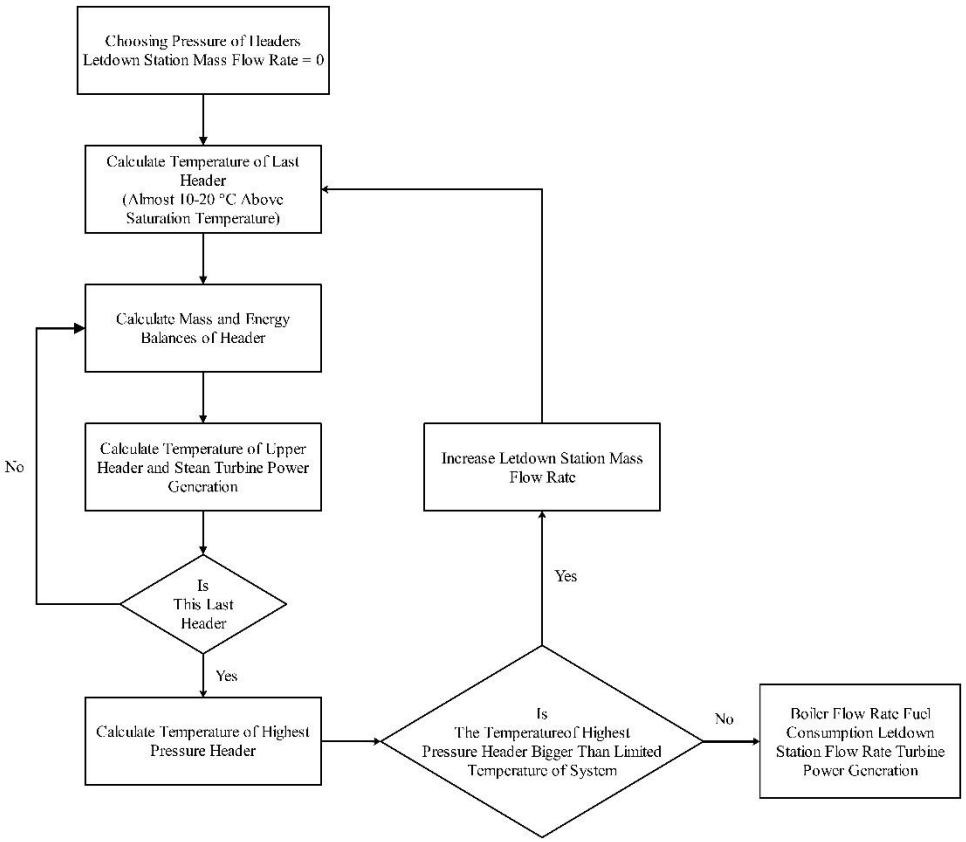

Figure 2: Algorithm flowchart for steam network targeting for the proposed cogeneration system in the steam network [39].

Some of the necessitated data for simulation of the steam network are listed in Table 5. Besides, Table 6 shows the mass flue rate of steam produced and consumed by the site-wide utility.

Table 5: Key inputs for simulation of the steam network [24]

Streams	Supply temperature $T_S\ (K)$	Target temperature, $T_T\ (K)$	Pressure, $P\ (kPa)$
VHP	384.15	823.15	10130
HP	378.15	543.15	4052
MP	378.15	505.15	2026
LP	378.15	445.15	506.5
CW	293.15	303.15	101.3

Table 6: Design considerations for simulation of the steam network [24]

Pressure of header	$\dot{m}_{Generation}$ $[kg.S^{-1}]$	$\dot{m}_{Consumption}$ $[kg.S^{-1}]$
VHP	0	0
HP	30.3	29.81
MP	22.6	50.05
LP	1.9	34.39

3.5. Key performance criterion

The target of the devised system of this study is proposing a hybrid polygeneration system integrated with a total site polygeneration system. Thus, there are other products in this system besides the heat and power that should be taken into account for computing efficiencies.

The energy efficiency of the standalone system as the topping cycle which is not integrated with SN operated by biogas and solar energy can be written as follows:

$$\eta_{en,standalone} = \frac{\dot{W}_{\text{Net,standalone}} + \dot{Q}_{DWH} + \dot{m}_{36} \times LHV_{CO2} + \dot{m}_{13} \times LHV_{H_2}}{\dot{m}_1 \times LHV_{biogas} + \dot{Q}_{field}} \quad (46)$$

$$\dot{W}_{\text{Net,standalone}} = \dot{W}_{el,GTC} + \dot{W}_{el,ORC} - \dot{W}_{el,CCS} - \dot{W}_{el,CO_2comp} - \dot{W}_{el,fuel\ comp} \quad (47)$$

Where LHV is lower heating value and $\dot{W}_{\text{Net,standalone}}$ represent the net power output of the standalone system. The energy efficiency of the proposed integrated cogeneration system with CCS and hydrogen production fueled by biogas, solar energy, and NG can be expressed as follows:

$$\eta_{en,cog} = \frac{\dot{W}_{Net,cog} + \dot{Q}_{DWH}\left(1 - \frac{T_0}{T_{DWH}}\right) + \dot{m}_{36} \times LHV_{CO2} + \dot{m}_{13} \times LHV_{H_2} + \dot{Q}_{Consumption}}{\dot{m}_1 \times LHV_{biogas} + \dot{Q}_{field} + \dot{m}_{NG} \times NHV_{NG} + \dot{Q}_{Generation}} \quad (48)$$

$\dot{W}_{Net,cog}$ in Eq. 49 is the net extracted power and is stated as:

$$\dot{W}_{Net,cog} = \dot{W}_{el,GTC} + \dot{W}_{el,ORC} + \dot{W}_{ST1} + \dot{W}_{ST2} + \dot{W}_{ST3} - \dot{W}_{el,CCS} - \dot{W}_{el,CO_2comp} - \dot{W}_{el,fuel\ comp} \quad (49)$$

$$\dot{Q}_{Consumption} = \sum_i \dot{Q}_{Consumption,i} \quad (49)$$

$$\dot{Q}_{Generation} = \sum_i \dot{Q}_{Generation,i} \quad (50)$$

Finally, the power/heating ratio for the cogeneration system can be expressed as:

$$R_{Cog} = \frac{\dot{W}_{Net,cog}}{\dot{Q}_{Consumption}} \quad (51)$$

4. Model Validation

In this study, the performance of the devised multi-generation system is established in Engineering Equation Solver (EES). The validity of this model is evaluated by reviewing the existing computational and experimental results found in the literature. In order to verify the model devised for the reformer, the predicted syngas composition is compared with the data reported by Su et al. [25] study (Table 7). CST-tower unit is validated by a comparison between the outlet temperature strategy of the fixed receiver in the present study, and Ref. [30] (Table 8). From these results, it can be concluded that a good correspondence is established between the model of this study and recent experimental data found in the literature.

Table 7: Verification of simulation results for the biogas reformer

Syngas composition (mol %)	Present study	Ref. [25]	Error [%]
H_2O	16.45	16.67	-1.3
H_2	51.97	51.72	0.4
CO	21.7	21.84	-0.6
CO_2	9.354	9.19	2.8
CH_4	0.5348	0.57	-3.6

Table 8: Verification of simulation results for CST-tower unit

CTS-tower design parameters	Present study	Ref. [30]	Error [%]
Heliostat field area (m^2)	296,640	296,468	0
Receiver surface area (m^2)	411	412	- 0.2
Receiver aperture area (m^2)	329	330	- 0.3
Receiver surface temperature (K)	780	770.5	1.2
Receiver efficiency (–)	0.913	0.89	2.5
Solar field mass flow rate of molten salt ($kg\ s^{-1}$)	338	343	-1.4

At last, the results of the simulation of the steam network are compared with those of Sun et al. [24]. The outcomes of this validation for mass flow rate and power are demonstrated in Tables 9 and 10, respectively. It can be concluded from this comparison that there is a good agreement between the results of the two studies.

Table 9: Verification of simulation results for the steam network (power calculation).

Pressure of header	Temperature of header (°C)			M_{Output} (kg S^{-1})		
	Sun et al. [24]	Present study	Error (%)	Sun et al. [24]	Present study	Error (%)
VHP	570	570	0	0	0	0
HP	378.6	382.3	0.98	26.4	29.81	12.92
MP	283.2	285.9	0.95	47	50.05	6.49
LP	171.8	171.9	0.06	33.9	34.39	1.44

Table 10: Verification of simulation results for the steam network (power calculation).

Steam turbine	Generated power (MW)		
	Sun et al. [24]	Present study	Error (%)
Steam turbine 1 (ST 1)	10.5	10.23	2.57
Steam turbine 2 (ST 2)	6.77	7.03	3.84
Steam turbine 3 (ST 3)	5.82	6.23	7.04

5. Results and discussions

5.1. Modeling results

Results of simulation for steam network targeting are illustrated in Fig. 3. In this simulation, it is assumed that the maximum steam temperature is 570℃. All determining parameters such as the mass flow rate, temperature, pressure, and output power of turbines are taken into account. It can be deduced from Fig. 4 that the heat recovery unit has a steam consumption rate of 51.35 kg/s, which is provided by products of Steam turbines 1, 2, and 3 are 11.05, 7.481, and 6.956 MW, respectively. 14.69 kg/s steam is generated subsequently.

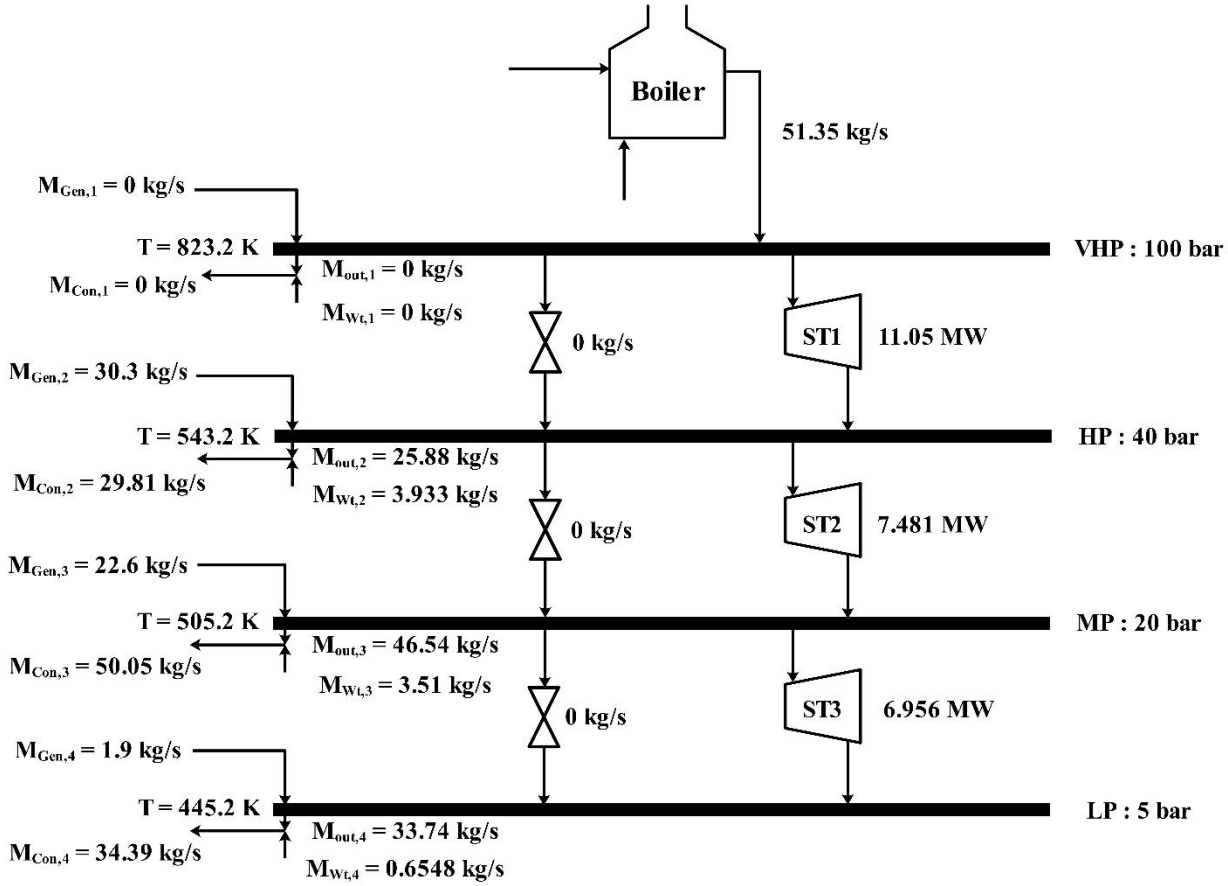

Figure 3: Results of simulation for steam network targeting for a maximum steam temperature of 570℃.

Along with Fig. 3, some of the other results of energy analysis of the devised system are listed in Table 11. It can be concluded that using the SN increases the energy efficiency by about 9% in comparison with systems is increased by approximately 9% compared to the standalone

multigeneration system. The devised system also has a heating load of 238.087 MW and net electricity of 57.634 MW, which makes it a suitable option for energy generation purposes (Table 11). The net electricity/heating ratio is also noticed in this study. The value of this variable is obtained at 0.2642, which shows that despite the surplus heating generated, the power generation still has superiority over heating.

Table 11: Final results obtained from simulation.

Parameter	Value
$\dot{W}_{GTC}$ (MW)	39.096
$\dot{W}_{ORC}$ (MW)	8.6
$\dot{W}_{Comp}$ (MW)	15.55
$\dot{m}_{Hydrogen}$ (kg/s)	0.3786
$\dot{m}_{CO2}$ (kg/s)	166.3
$\dot{Q}_{Consumption}$ (MW)	238.087
$\dot{W}_{Net,standalone}$ (MW)	32.147
$\dot{W}_{Net,cog}$ (MW)	57.634
$\eta_{en,standalone}$ (%)	51.72
$\eta_{en,cog}$ (%)	60.55
R_{Cog}	0.2642

5.2. Parametric study

In this sub-section, the impact of main parameters on the energy efficiency and power/heat ratio is investigated through a parametric study. The considered chief parameters include biogas flowrate, operating conditions of the reformer (T_r and P_r), and pressure of headers in the SN unit.

5.2.1. Biogas flowrate

The impact of biogas flowrate on the net power/heat ratio and energy efficiency is demonstrated in Fig. 4. According to Fig. 4, as the biogas flow rate goes up, the net power/heat ratio is increased. While the biogas flow rate changes from 5 to 15 kg/s, the net electricity of the power cycles increases by 86.6%. On the contrary, the net electricity of the steam network shows no alteration and remains constant. The reason is that the $Q_{consumption}$ in the steam network is not dependent on the biogas flowrate alterations. It can be concluded from this figure that with rising up of the net power/heat ratio, the energy efficiency declines exponentially and goes from 78.63% to 49.86%. The explanation could be as follows: when the biogas flow rate increases, the input heat energy increases too -similar to output work; but as the ratio of input increase is higher, energy efficiency is dropped.

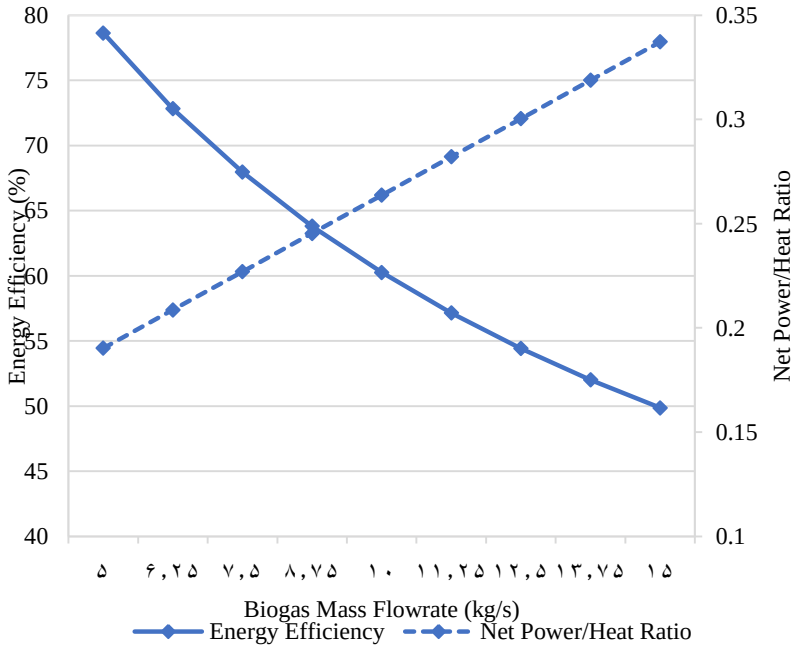

Figure 4: Effect of the biogas flowrate on energy efficiency and power/heat ratio

5.2.2. Reformer temperature

For this investigation, the temperature of the reformer is changed from 923 to 1173 K, and other parameters are considered constant. The impact of the reformer temperature on energy efficiency and net power/heat ratio is shown in Fig. 5. It can be seen that both of these parameters decrease as the reformer temperature goes up. However, the reduction rates are different since the net power/heat ratio decreases at a higher pace than the energy efficiency. This observation can be explained as follows. The net electricity of the

power cycles decreases as the reformer temperature goes up. In this temperature range, the output power decreases by 17.2%. Besides, the generated heat for heating purposes declines about 42.5% resulting in a net power/heat ratio decrease.

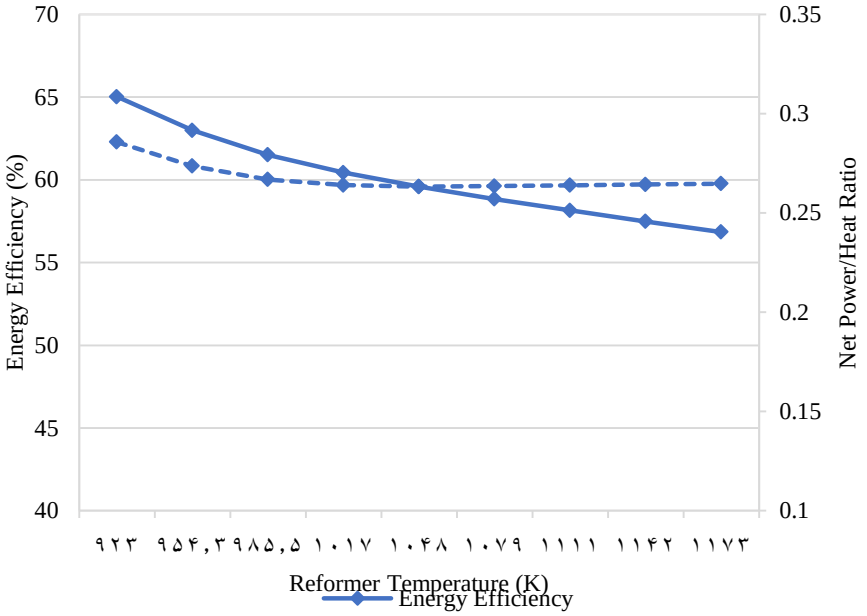

Figure 5: Effect of the reformer temperature on energy efficiency and power/heat ratio

5.2.3. Reformer Pressure

To analyze the impact of the reformer pressure on energy efficiency and net power/heat ratio, the biogas pressure is increased 6 bar from 1 to 7 bar, while other parameters have remained unvaried (Fig. 6). The generated power increases with the increase of the reformer pressure. Because of the increase in the reformer pressure, the generated power of the cycles increases by 28.4%. In the meantime, carbon capturing increases considerably, while the production of hydrogen decreases about 31.4%.

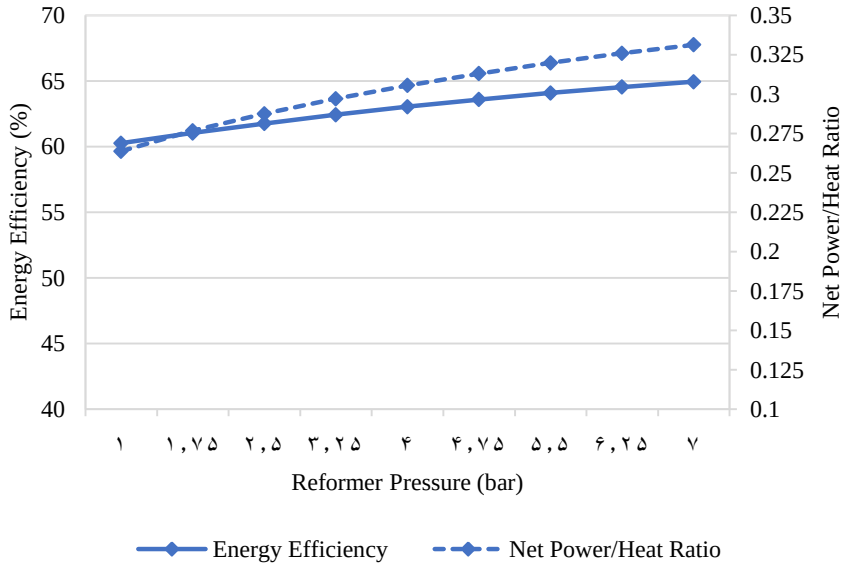

Figure 7: Effect of the reformer pressure on energy efficiency and power/heat ratio

5.2.4. Steam network medium pressure

Based on analyzing the results shown in Fig. 8, it can be concluded that with increasing P_{MP}, both the energy efficiency and net power/heat ratio are

decreased. According to this figure, by increasing P_{MP} from 15 bar to 25 bar, energy efficiency decreases about 1.5% and reaches 59.7%. The net power/heat ratio also is reduced and goes from 0.269 to 0.257. The following reasons can describe these trends. When P_{MP} is increased, expansion ratios of upper turbines decrease, and therefore the power of steam turbines and heating load are lowered. This process results in a decrease in energy efficiency and R_{Cog}, because of the higher role of net electricity.

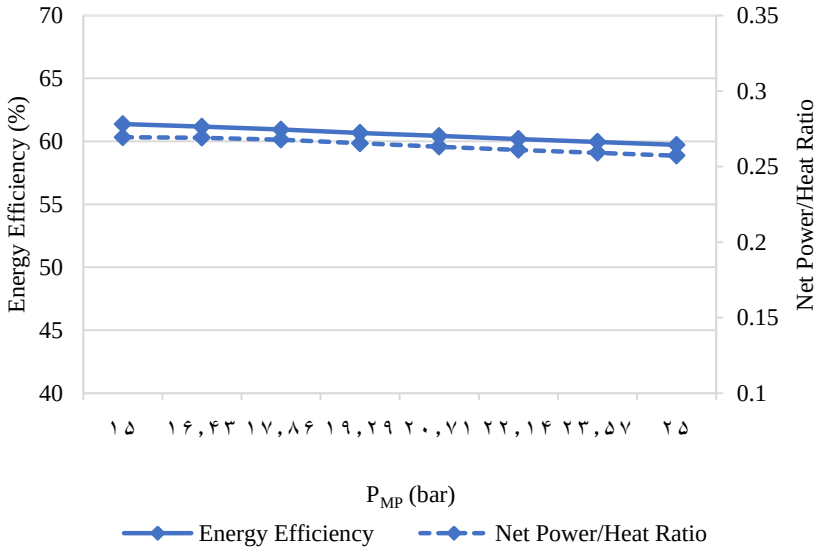

Figure 8: Impact of the steam network medium pressure on the net power/heat ratio and energy efficiency

5.2.5. Steam network high pressure

The impact of steam network very high pressure on energy efficiency and net power/heat ratio can be deduced from Fig. 9. Based on this figure, an increase of the high-pressure results in a decrease of both of these parameters. When the high pressure is increased by 2 bar and reaches 5 bar, the energy efficiency is slightly decreased by 1.5% and goes to 59.7%. net power/heat ratio goes from 0.267 to 0.260. The following reasons can be enumerated for such a trend. As HP rises up, the power of steam turbines decreases along with the heating load; accordingly, the net power/heating ratio declines.

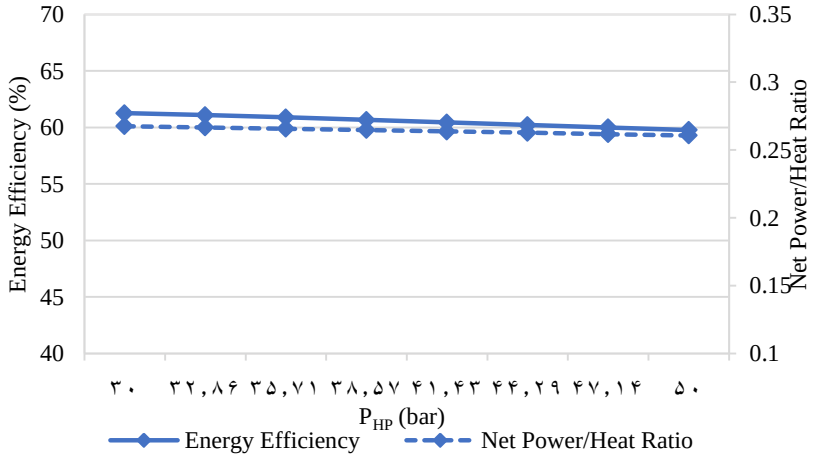

Figure 9: Effect of the steam network high pressure on energy efficiency and power/heat ratio

5.2.6. steam network Very high pressure

Fig. 10 is a depiction of the impact of the steam network's very high pressure on energy efficiency and net power/heat ratio. It can be concluded from this figure that both of the parameters mentioned above decrease with the increase of very high pressure. As the energy efficiency goes smoothly from 61.2 to 59.7 %, the net power/heat ratio is not changing noticeably. It is worthy of pinpointing that the heating load and power of GTC and ORC

unit have remained unvaried through this analysis, and hence the trend of the net electricity of the devised multi-generation system, R_{Cog}, and energy efficiency follows that of the steam turbine's power.

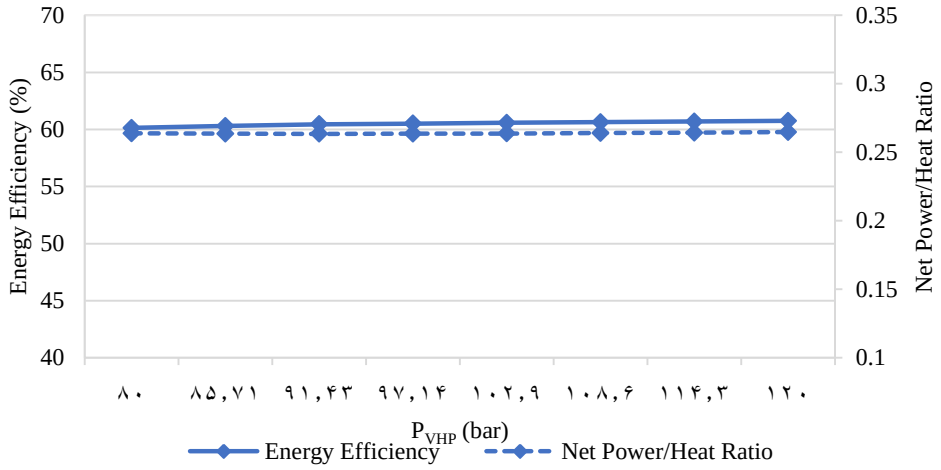

Figure 10: Effect of the steam network very high pressure on energy efficiency and power/heat ratio

6. Conclusions

In this study, an innovative multi-generation energy system based on biogas and solar energy is proposed. Besides, this system also is devised for hydrogen concurrently benefited from a CCS unit and also is designed for site-wide utility for heat recovery and heat and power generation for meeting the necessitated energy of the system. In order to produce the steam needed in the SN unit, NG is utilized as a primary fuel. Solar thermal energy, absorbed by a CTS-tower plant, is utilized in the processes which are taken place in the reformer. The necessitated heat for steam is made available through these processes. Furthermore, CO_2 and H_2 of the reformer exhaust syngas are retrieved by CCS and PSA, respectively. In this study, the energetic analysis is carried out on the devised system. Biogas flowrate, reformer temperature, reformer pressure, and steam network in the medium, high, and very high-pressure levels are among the parameters analyzed in this study. The following is the summary of the final results:

- The efficiency is increased from 51.72% to 60.55% through the integration of the steam network system with the topping system.
- Consequently, an increase from 32.147 MW to 57.634 MW is seen in the net power.
- A decrease in CO_2 conversion is visible when the reformer temperature is increased.
- As the reformer pressure rose up, overall net power output and captured carbon dioxide increases, respectively.
- Adjusting the reformer pressure design is a solution for maximizing the net power/heat ratio.
- These alterations increase the devised system efficiency: decreasing biogas flow rate, reformer temperature, P_{MP}, or P_{HP} of the SN unit. Also, increasing reformer pressure and P_{VHP} of the SN unit increases energy efficiency.

References

[1] M. D. Madvar, F. Ahmadi, R. Shirmohammadi, and A. J. E. R. Aslani, "Forecasting of wind energy technology domains based on the technology life cycle approach," vol. 5, pp. 1236-1248, 2019.

[2] M. Ebadollahi, H. Rostamzadeh, O. Pourali, H. Ghaebi, and M. Amidpour, "Inherently safety design of a dual-loop bi-evaporator combined cooling and power system: 4E and safety based optimization approach," *Process Safety and Environmental Protection,* vol. 154, pp. 393-409, 2021/10/01/ 2021.

[3] H. Nasrollahi, F. Ahmadi, M. Ebadollahi, S. Najafi Nobar, and M. Amidpour, "The greenhouse technology in different climate conditions: A comprehensive energy-saving analysis," *Sustainable Energy Technologies and Assessments,* vol. 47, p. 101455, 2021/10/01/ 2021.

[4] M. Ebadollahi, H. Rostamzadeh, M. Z. Pedram, H. Ghaebi, and M. Amidpour, "Proposal and assessment of a new geothermal-based multigeneration system for cooling, heating, power, and hydrogen production, using LNG cold energy recovery," *Renewable Energy,* vol. 135, pp. 66-87, 2019/05/01/ 2019.

[5] M. Mohsenipour, F. Ahmadi, A. Mohammadi, M. Ebadollahi, and M. Amidpour, "Investigation of a Geothermal-Based CCHP System from Energetic, Water Usage and CO2 Emission Viewpoints," *Gas Processing Journal,* vol. 7, no. 1, pp. 41-52, 2019.

[6] M. Ebadollahi, H. Rostamzadeh, P. Seyedmatin, H. Ghaebi, and M. Amidpour,

"Thermal and exergetic performance enhancement of basic dual-loop combined cooling and power cycle driven by solar energy," *Thermal Science and Engineering Progress,* vol. 18, p. 100556, 2020/08/01/ 2020.

[7] A. Buonomano, F. Calise, A. Palombo, and M. Vicidomini, "BIPVT systems for residential applications: An energy and economic analysis for European climates," *Applied Energy,* vol. 184, pp. 1411-1431, 2016/12/15/ 2016.

[8] C. Renno, D. D'Agostino, F. Minichiello, F. Petito, and I. Balen, "Performance analysis of a CPV/T-DC integrated system adopted for the energy requirements of a supermarket," *Applied Thermal Engineering,* vol. 149, pp. 231-248, 2019/02/25/ 2019.

[9] S. Ghorbani and M. H. J. G. P. J. Khoshgoftar Manesh, "Conventional and Advanced Exergetic and Exergoeconomic Analysis of an IRSOFC-GT-ORC Hybrid System," vol. 8, no. 1, pp. 1-16, 2020.

[10] A. Mosaffa, Z. Ghaffarpour, and L. G. J. S. E. Farshi, "Thermoeconomic assessment of a novel integrated CHP system incorporating solar energy based biogas-steam reformer with methanol and hydrogen production," vol. 178, pp. 1-16, 2019.

[11] A. Ebrahimi, B. Ghorbani, M. Ziabasharhagh, and M. J. Rahimi, "Biomass gasification process integration with Stirling engine, solid oxide fuel cell, and multi-effect distillation," *Journal of Thermal Analysis and Calorimetry,* 2020/10/17 2020.

[12] A. Ebrahimi, B. Ghorbani, and M. Ziabasharhagh, "Pinch and sensitivity analyses of hydrogen liquefaction process in a hybridized system of biomass gasification plant, and cryogenic air separation cycle," *Journal of Cleaner Production,* vol. 258, p. 120548, 2020/06/10/ 2020.

[13] V. P. Rathod, J. Shete, and P. V. Bhale, "Experimental investigation on biogas reforming to hydrogen rich syngas production using solar energy," *International Journal of Hydrogen Energy,* vol. 41, no. 1, pp. 132-138, 2016.

[14] A. Iulianelli, S. Liguori, Y. Huang, and A. Basile, "Model biogas steam reforming in a thin Pd-supported membrane reactor to generate clean hydrogen for fuel cells," *Journal of Power Sources,* vol. 273, pp. 25-32, 2015.

[15] A. Mouaky and A. Rachek, "Energetic, exergetic and exergeoeconomic assessment of a hybrid solar/biomass poylgeneration system: A case study of a rural community in a semi-arid climate," *Renewable Energy,* Article vol. 158, pp. 280-296, 2020.

[16] J. Hernández-Santoyo and A. Sánchez-Cifuentes, "Trigeneration: an alternative for energy savings," *Applied Energy,* vol. 76, no. 1-3, pp. 219-227, 2003.

[17] G. Chicco and P. Mancarella, "Distributed multi-generation: a comprehensive view," *Renewable and sustainable energy reviews,* vol. 13, no. 3, pp. 535-551, 2009.

[18] V. Ghazizadeh, B. Ghorbani, R. Shirmohammadi, M. Mehrpooya, and M. H. Hamedi, "Advanced Exergoeconomic Analysis of C3MR, MFC and DMR Refrigeration Cycles in an Integrated Cryogenic Process," *Gas Processing,* vol. 6, no. 1, pp. 41-71, 2018.

[19] H. Golchoobian, M. Amidpour, and O. Pourali, "Thermodynamic analysis of three combined power and refrigeration Systems based on a demand," *Gas Processing,* vol. 6, no. 1, pp. 29-40, 2018.

[20] J. Wang, Z. Yan, M. Wang, Y. Song, and Y. Dai, "Parametric analysis and optimization of a building cooling heating power system driven by solar energy based on organic working fluid," *International Journal of Energy Research,* vol. 37, no. 12, pp. 1465-1474, 2013.

[21] M. Shariati and M. Amidpour, "Development of an Integrated Structure of CHP and Heavy Hydrocarbons Liquids Using Fischer-Tropsch Synthesis," *Gas Processing,* vol. 4, no. 2, pp. 32-44, 2016.

[22] É. S. Van-Dal and C. Bouallou, "Design and simulation of a methanol production plant from CO2 hydrogenation," *Journal of Cleaner Production,* vol. 57, pp. 38-45, 2013.

[23] Y. Cao, Y. Gao, Y. Zheng, and Y. Dai, "Optimum design and thermodynamic analysis of a gas turbine and ORC combined cycle with recuperators," *Energy Conversion and Management,* vol. 116, pp. 32-41, 2016.

[24] L. Sun, S. Doyle, and R. Smith, "Heat recovery and power targeting in utility systems," *Energy,* vol. 84, pp. 196-206, 2015/05/01/ 2015.

[25] B. Su, W. Han, and H. Jin, "Proposal and assessment of a novel integrated CCHP system with biogas steam reforming using solar energy," *Applied energy,* vol. 206, pp. 1-11, 2017.

[26] I. Uehara, "Separation and purification of hydrogen," *Energy carriers and conversion systems with emphasis on hydrogenvol,* vol. 1, pp. 268-82, 2008.

[27] D.-K. Moon, Y. Park, H.-T. Oh, S.-H. Kim, M. Oh, and C.-H. Lee, "Performance analysis of an eight-layered bed PSA process for H2 recovery from IGCC with pre-combustion carbon capture," *Energy Conversion and Management,* vol. 156, pp. 202-214, 2018/01/15/ 2018.

[28] A. Pirmohamadi, H. Ghaebi, B. M. Ziapour, and M. Ebadollahi, "Exergoeconomic Analysis of a Novel Hybrid System by Integrating the Kalina and Heat Pump Cycles with a Nitrogen Closed Brayton System," *Energy Reports,* vol. 7, pp. 546-564, 2021/11/01/ 2021.

[29] M. Ebadollahi, H. Rostamzadeh, O. Pourali, H. Ghaebi, and M. J. J. o. E. R. T. Amidpour, "Close supercritical versus inverse

Brayton cycles for power supply, using waste of a biogas-driven open Brayton cycle," vol. 143, no. 9, p. 092102, 2021.
[30] S. S. M. Tehrani and R. A. Taylor, "Off-design simulation and performance of molten salt cavity receivers in solar tower plants under realistic operational modes and control strategies," *Applied energy,* vol. 179, pp. 698-715, 2016.
[31] X. Li, W. Kong, Z. Wang, C. Chang, and F. Bai, "Thermal model and thermodynamic performance of molten salt cavity receiver," *Renewable energy,* vol. 35, no. 5, pp. 981-988, 2010.
[32] M. Binotti, M. Astolfi, S. Campanari, G. Manzolini, and P. Silva, "Preliminary assessment of sCO2 power cycles for application to CSP Solar Tower plants," *Energy Procedia,* vol. 105, pp. 1116-1122, 2017.
[33] U. Izquierdo *et al.*, "Biogas steam and oxidative reforming processes for synthesis gas and hydrogen production in conventional and microreactor reaction systems," *International Journal of Hydrogen Energy,* vol. 37, no. 18, pp. 13829-13842, 2012.
[34] A. Vita *et al.*, "Methanol synthesis from biogas: A thermodynamic analysis," *Renewable Energy,* vol. 118, pp. 673-684, 2018.
[35] M. Taheri, A. Mosaffa, and L. G. Farshi, "Energy, exergy and economic assessments of a novel integrated biomass based multigeneration energy system with hydrogen production and LNG regasification cycle," *Energy,* vol. 125, pp. 162-177, 2017.
[36] Z. Ghaffarpour, M. Mahmoudi, A. Mosaffa, and L. G. Farshi, "Thermoeconomic assessment of a novel integrated biomass based power generation system including gas turbine cycle, solid oxide fuel cell and Rankine cycle," *Energy conversion and management,* vol. 161, pp. 1-12, 2018.
[37] P. Ahmadi and I. Dincer, "Thermodynamic analysis and thermoeconomic optimization of a dual pressure combined cycle power plant with a supplementary firing unit," *Energy Conversion and Management,* vol. 52, no. 5, pp. 2296-2308, 2011.
[38] L. Sun and R. Smith, "Performance modeling of new and existing steam turbines," *Industrial & Engineering Chemistry Research,* vol. 54, no. 6, pp. 1908-1915, 2015.
[39] H. Nikoomaram, M. Amidpour, M. Panahi, and A. Farhang Sotoodeh, "Developing an integrated hybrid polygeneration system combined with utility steam network," *International Journal of Sustainable Energy,* pp. 1-29, 2021.